LAWRENCE
LIVERMORE
NATIONAL
LABORATORY

LLNL-JRNL-603073

# PHASE TRANSFORMATION B1 TO B2 IN TITANIUM AND ZIRCONIUM CARBIDES AND NITRIDES UNDER PRESSURE

V. I. Ivashchenko, P. E. A. Turchi, V. I. Shevchenko

November 19, 2012

Computational Materials Physics

## Disclaimer

# Phase transformation B1 to B2 in titanium and zirconium carbides and nitrides under pressure

V. I. Ivashchenko[1], P. E. A. Turchi[2], V. I. Shevchenko[1]

[1]*Institute of Problems of Material Science, NAS of Ukraine, Krzhyzhanosky str. 3, 03142 Kyiv, Ukraine*
[2]*Lawrence Livermore National Laboratory (L-352), P.O. Box 808, Livermore, CA 94551, USA*

**Abstract**

Phase stability of various phases of MX (M=Ti, Zr; X=C, N) at equilibrium and under pressure is examined based on first-principles calculations of the electronic and phonon structures. The results reveal that all B1 (NaCl-type) MX structures undergo a phase transition to the B2-structures under high pressure in agreement with previous total-energy calculations. The B1-MX structures are dynamically stable under very high pressure (210-570 GPa). The pressure-induced B2 (CsCl-type) MC phases are dynamically unstable even at high pressures, and TiN and ZrN are found to crystallize with the B2-structure only at pressures above 55 GPa. The first-order B1-to-B2 phase transition in these nitrides is not related to the softening of phonon modes, and the dynamical instability of B2-MX is associated to a high density of states at the Fermi level.

## 1. Introduction

Transition metal compounds (TMC) form a class of materials with the NaCl-type crystal structure (B1) in a wide composition range, and exhibit extremely high melting points, hardness, and metallic conductivity [1,2]. These materials are exploited under extreme conditions (high temperature, high pressure, *etc*.), and they are widely used as main layers in ultra-hard nano-composite coatings [3]. Therefore, it is important to understand the peculiarities of their behavior under extreme conditions. In this investigation we focus on titanium and zirconium carbides and nitrides (MX, M=Ti, Zr; X=C, N) that crystallize with the NaCl-type (B1) lattice since their high-pressure stability is not very well known. To our knowledge, there has been only several works devoted to this problem: Dubrovinskaia *et al*. observed a B1-R phase transition in TiC at pressure above 18 GPa [4], although Winkler *et al*. found no phase transition in the B1 titanium carbide up to 26 GPa [5]. On the other hand, many theoretical studies predict the B1 to B2 (CsCl-type) phase transition in MX, under high pressure. In Table I, we report the transition pressures ($P_0$) obtained in the present investigation and from other studies based on first-principles and empirical-potential calculations. It is seen that all the first-principles and three-body potential calculations provide consistent values of $P_0$, whereas the neglect of three-

body interactions in the empirical-potential studies leads to much lower values of $P_0$ (cf. Table I). Based on the total-energy calculations for TiC Zhao *et al.* predicted two phase transition paths under pressure: B1 → (117 GPa) TlI' → (172 GPa) TlI, and/or B1 → (131 GPa) TiB' → (148 GPa) TiB [6]. Note that a description of these phases can be found in Ref. [6].

It follows from this brief review that many theoretical investigations predict a B1 to B2 phase transition in MX under pressure in the range of 200-550 GPa. Also, the more complex cubic to orthorhombic transformations under pressure in TiC and ZrC were predicted in some first-principles calculations. For MX, there are no any experimental evidences of the existence of other structural polytypes, besides the B1 structure, in a wide range of temperatures (up to melting points) and pressures.

The main goal of this paper is to verify the dynamical stability of the B2-MX phases under pressure, and to investigate other plausible phases of MX.

The paper is organized as follows. In Sec. 2 we present our theoretical framework and the computational details. Sec. 3 contains the results of our calculations together with comments. Finally, Sec. 4 contains the main conclusions.

## 2. Methodology

A first-principles pseudo-potential method was used to investigate different phases of MX (M=Ti, Zr; X=C, N). Scalar-relativistic band-structure calculations within density functional theory (DFT) were carried. The "Quantum-ESPRESSO" first-principles code [14] was used to perform the pseudo-potential calculations, with Vanderbilt ultra-soft pseudo-potentials to describe electron-ion interactions [15]. In the Vanderbilt approach [15], the orbitals are allowed to be as soft as possible in the core region so that their plane-wave expansion converges rapidly. For Ti and Zr atoms, the semi-core states were treated as valence states. Plane waves up to a kinetic energy cutoff of 38 Ry (516.8 eV) were included in the basis set. The exchange-correlation potential was treated in the framework of the generalized gradient approximation (GGA) of Perdew-Burke-Ernzerhof (PBE) [16]. Brillouin-zone integrations were performed using sets of special k-points corresponding to the (8 8 8) Monkhorst-Park mesh [17]. For the 8-atom cell of the TlI-type TiC, we used a (8 4 8) mesh that, although it generates a lower number of k-points, provides an acceptable accuracy. Each eigenvalue was convoluted with a Gaussian with width $\sigma$=0.02 Ry (0.272 eV). All structures were optimized by simultaneously relaxing the atomic basis vectors and the atomic positions inside the unit cells using the Broyden-Fletcher-Goldfarb-Shanno (BFGS) algorithm [18]. The relaxation of the atomic coordinates and the unit cell was considered to be complete when the atomic forces were less than 1.0 mRy/Bohr (25.7 meV/Å), the stresses were smaller than 0.025 GPa, and the total energy during the structural

optimization iterative process was varying by less than 0.1 mRy (1.36 meV). The crystalline and energetic parameters of various phases of titanium and zirconium carbides and nitrides after structural optimization are summarized in Table II. The electronic densities of states (DOS) were calculated using the (12 12 12) mesh.

The above-described pseudo-potential procedure was used to study the phonon spectra of the NaCl (B1) and CsCl (B2) -type MX compounds in the framework of the density-functional perturbation theory (DFPT) described in Refs. [14,19]. The first-principles DFPT calculations were carried out for a (8 8 8) q-mesh, and then the phonon densities of states (PHDOS) were computed using a (12 12 12) q-mesh by interpolating the computed phonon dispersion curves. Both the DOS and PHDOS were calculated with the tetrahedron method implemented in the "Quantum-ESPRESSO" code [14].

To check the acceptability of the chosen conditions for the calculations we estimate the heat of formation of B1-MX, $H^f$, using the expression $H^f = E_{tot} - \sum n_i E_i$, where $E_{tot}$ is the total energy of the bulk compound with $n_i$ atoms of all involved elements $i$ (Ti, Zr, C, and N), and $E_i$ is the total energy of the bulk hexagonal close-packed structure for Ti or Zr (space group $P6_3/mmc$, No. 194) and diamond (A4) for C, and half the total energy of $N_2$ molecule for N, respectively. The total energy and equilibrium bond length of $N_2$ molecule were computed using the extended two-atom cubic cell. The bond length of $N_2$ molecule was in agreement with experiment (1.098 Å) within 1%. The computed values of $H^f$ for NaCl-type (B1) TiC, TiN, ZrC and ZrN are summarized in comparison with the corresponding experimental and theoretical values from other studies. We note that although theoretical formation energies are fairly consistent with each other, they are all somewhat higher than the experimentally determined values. One plausible reason for such a discrepancy for zirconium carbide and nitride was discussed in Ref. [29].

The reliability of the DFPT calculations of TMC was proved in Ref. [30]. Here we only compare the calculated phonon spectrum with the experimental dispersion curves for TiN [31] to confirm that the DFPT results correctly reproduces the anomalies in the phonon spectra for TMC.

## 3. Results and Discussion

To predict possible stable structures of MX, at first we performed total energy calculations for different phases of TiC and TiN that were identified for other binary compounds (NbN, WC, MoC, CoSn, CsCl, NiAs, ZnS, *etc*.) at equilibrium [1,2]. The structural and energetic characteristics of the most stable phases of TiC and TiN are summarized in Table II. It is worth

noting that B1 is among all the calculated structures the most stable, and a good agreement exists between the computed and experimental structural parameters shown in Table II.

In order to predict possible stable phases of TiC and TiN under high pressure we calculated the total energies ($E_T$) of all the TiC and TiN phases presented in Table III as functions of cell volume (V). An analysis of the calculated volume dependence of the total energies, $E_T(V)$, enabled us to identify only the CsCl-type structures that could be derived from the B1-phases at high pressure. Under this circumstance, for ZrC and ZrN, we performed total-energy calculations for only two phases with the NaCl (B1) and CsCl (B2) -type structures (cf. I). We did not found any stable orthorhombic phase of TiC at pressure, as was predicted in Ref. [6]: the TiB-type TiC phase automatically transformed to the B1 structure during static relaxation, and the B1-type TiC did not transform into the TlI-type TiC under pressure, although the latter structure was quite stable at equilibrium (cf. Table II). Such a discrepancy in the prediction of new phases in TiC is attributed to an inappropriate procedure of geometry optimization used in Ref. [6].

The total energies as functions of cell volume and enthalpies as functions of pressure for the B1- and B2- phases are shown in Fig. 1. One can see that, for the MX phases, the B1-to-B2 first-order phase transition takes place at high pressure. The calculated values of transition pressure ($P_0$) are presented in Table I, where, for comparison, the values of $P_0$ obtained from other first-principles and empirical-potential calculations are also shown. It is seen that all calculated characteristics agree well except for $P_0$ calculated from the two-body empirical potential approach [8,10,13]. It is likely that the lower values of $P_0$ in this approach are a consequence of the neglect of the many-body interactions.

With the B1-to-B2 phase transitions in MX under pressure now established, we need to verify that the new pressure-induced phases are dynamically stable. To address this issue, we calculated the phonon dispersion curves along some high-symmetry directions of **k**-space for the B1- and B2-phases of MX at equilibrium and under pressure $P \geq P_0$. The calculated phonon spectra are shown in Fig. 2. We note that the phonon spectra of all B1-phases do not contain any soft modes, which means that theses phases will be dynamically stable up to very high pressures. On the contrary, a softening of the acoustic phonon modes around the X and M points is observed in the phonon spectrum of the B2-structures at equilibrium, which implies that these phases are dynamically unstable. For TiC and ZrC, the condensed phonon modes are preserved even at high pressures (cf. Figs. 2 a, c). On the other hand the titanium and zirconium nitrides with the B2 (CsCl-type) structure can be stabilized by applying high pressure. In Fig. 3 we show the dependence of the soft $M_{4^-}$ modes on pressure for TiN and ZrN, and clearly the phonon anomalies in these nitrides disappear at $P > 55$ GPa.

To understand the plausible origin of the dynamical instability of the B2 MX phases, let us investigate the electronic structure of the B1 and pressure-induced B2 phases. The densities of states (DOS) of the B1- and B2- MX phases at equilibrium are shown in Fig. 4. In the case of B1 MX, in increasing energy, the lowest bands are associated with the 2s states of X, then the next bands originate from X 2p- and M 3d –states, and finally, the broad M d-bands with a small admixture of X 2p states are located above the minimum of the DOS. There is a new type of M-$d_\gamma$ – M-$d_\gamma$ interactions in B2-based structures that are lacking in B1 MX. As a result, several local peaks appear at the bottom of the metal band. One can see that, for all the B2 MX phases, the Fermi level ($E_F$) crosses the local DOS maximum in a region of the spectrum formed by the M-$d_\gamma$ states (the partial DOS is not shown here). A high DOS at the Fermi level is usually associated with a structural instability and the existence soft phonon modes in the long-wave region, and the collapse of these modes leads to a structural transformation. Thus, the high DOS at the Fermi level identified in the case of B2 MX can be one of the reasons for the dynamical instability of these phases.

As a final note, since modern high-pressure devices can generate pressures up to 550 GPa that are higher than the maximum pressure of the earth's core (360 GPa) [32], we hope that our theoretical findings will motivate further high-pressure experiments to establish new pressure-induced phases in transition metal compounds including those that were examined in this work.

## CONCLUSIONS

Phase stability of various phases of MX (M=Ti, Zr; X=C, N) at equilibrium and under pressure was examined on the basis of first-principles calculations of the electronic and phonon structures. The calculated formation energies are in good agreement with the corresponding experimental values. The analysis of the dependencies of enthalpy and phonon spectra on pressure for these phases enabled us to bring the following conclusions.

It follows from the total energy calculations that all B1 MX structures undergo a phase transformation to the B2-structures under high pressure in agreement with previous total-energy calculations. The B1 MX structures are dynamically stable under very high pressure (209-570 GPa). The calculated phonon spectra show that the B2 MX compounds have collapsed acoustic modes at ambient and high pressures. However B2-based TiN and ZrN can be dynamically stabilized at pressures above 55 GPa. The first-order B1-to-B2 phase transition in these nitrides is not related to a softening of the phonon modes. For B2 MX, a high density of states at the Fermi level may be responsible for the dynamical instability of these phases.

**Acknowledgments**

This work was supported by the STCU Contract No. 5539. The work of P.T. was performed under the auspices of the U. S. Department of Energy by the Lawrence Livermore National Laboratory under contract No. DE-AC52-07NA27344.

**References**

[1] L.E. Toth, *Transition Metal Carbides and Nitrides* (Academic, New York, 1971).

[2] G.V. Samsonov and I.M. Vinitskii, *Handbook of Refractory Compounds* (Plenum, New York, 1980), 555 p.

[3] S. Veprek, J. Nanosci. Nanotechnol. **11**, 14 (2011).

[4] N.A. Dubrovinskaia, L.S. Dubrovinsky, S.K. Saxena, R. Ahuja, and B. Johansson, J. Alloys Compd. **289**, 24 (1999).

[5] B. Winkler, E.A. Juarez-Arellano, A. Friedrich, L. Bayarjargal, J.Y. Yan, and S.M. Clark, J. Alloys Compd. **478**, 392 (2009).

[6] Z. Zhao, X.-F. Zhou, L.-M. Wang, B. Xu, J. He, Z. Liu, H.-T. Wang, and Y. Tian, Inorg. Chem. **50**, 9266 (2011).

[7] R. Ahuja, O. Eriksson, J.M. Wills, and B. Johansson, Phys Rev B. **53**, 3072 (1996).

[8] P. Ojha, M. Aynyas, and S.P. Sanyal, Optoelectronics and Advanced Materials – Rapid Communications **2**, 50 (2008).

[9] K. Liu, X.-L. Zhou, H.-H. Chen, L.-Y. Lu, J. Therm. Anal. Calorim. DOI 10.1007/s10973-011-1927-5.

[10] P. Ojha, M. Aynyas, and S.P. Sanyal, J. Phys. Chem. Solids **80**, 148 (2007).

[11] R. Chauhan, S. Singh, and R.K. Singh, Cent. Eur. J. Phys. **6**, 277 (2008).

[12] A. Hao, T. Zhou, Y. Zhu, X. Zhang, R. Liu, Materials Chemistry and Physics **129**, 99 (2011).

[13] P. Ojha, M. Aynyas, and S.P. Sanyal, Cent. Eur. J. Phys. **7**, 102 (2009).

[14] S. Baroni, A. Dal Corso, S. de Gironcoli, P. Giannozzi, C. Cavazzoni, G. Ballabio, S. Scandolo, G. Chiarotti, P. Focher, A. Pasquarello, K. Laasonen, A. Trave, R. Car, N. Marzari, and A. Kokalj, http://www.pwscf.org (2011).

[15] D. Vanderbilt, Phys. Rev. B **41**, 7892 (1990).

[16] J.P. Perdew, K. Burke, and M. Ernzerhof, Phys. Rev. Lett. **77**, 3865 (1996**)**.

[17] H.J. Monkhorst and J.D. Pack, Phys. Rev. B **13,** 5188 (1976).

[18] S.R. Billeter, A. Curioni, and W. Andreoni, Comput. Mater. Sci. **27**, 437 (2003).

[19] S. Baroni, S. De Gironcoli, A. Dal Corso, and P. Gianozzii, Rev. Mod. Phys. **73**, 515 (2001).

[20] D.L. Vrel, J.-M. Lihrmann, and J.-P. Petitet, J. Chem. Eng. Data **40**, 280 (1995).

[21] Y.Yang, H.Lu. C. Yu, and J.M. Chen, J. Alloys Compd. **485**, 542-547 (2009).

[22] *Handbook of Chemistry and Physics,* edited by R.C. Weast, M.J. Astle, and W.H. Beyer (Chemical Rubber Co., Boca Raton, 1988), Vol. **69**.

[23] C.-S. Chen, C.-P. Liu, H.-G. Yang, and C.Y.A. Tsao, J. Vac. Sci. Technol. B **22**, 1075-1083 (2004).

[24] S. Hao, B. Delley, and C. Stampfl, Phys. Rev. B **74**, 035402 (2006).

[25] C. Stampfl, W. Mannstadt, R. Asahi, and A.J. Freeman, Phys. Rev. B **63**, 155106 (2001).

[26] A. F. Guillermet, J. Alloys Compd. **217**, 69 (1995).

[27] J. Li, D. Liao, S. Yip, R. Najafabadi, and L. Ecker, J. Appl. Phys. **93**, 9072 (2003).

[28] H.W. Hogosson, O. Eriksson, U. Jansson, and B. Johansson, Phys. Rev. B **63**, 134108 (2001).

[29] S. Kim, I. Szlufarska, and D. Morgan, J. Appl. Phys. **107**, 053521 (2010).

[30] E.I. Isaev, S.I. Simak, I.A. Abrikosov, R. Ahuja, Yu. Kh. Vekilov, M.I. Katsnelson, A.I. Lichtenstein, and B. Johansson, J. Appl. Phys. **101**, 123519 (2007).

[31] W. Kress, P. Roedhammer, H. Bilz, W.D. Teuchert, and A.N. Christensen, Phys. Rev. B **17**, 111 (1978).

[32] J.A. Xu, H.K. Mao, and P.M. Bell, Science **232**, 1404 (1986).

Table I. Transition pressures associated with the B1→B2 phase transformation for MX according to different electronic structure methods.

| Phase | $P_0$ | Procedure | Reference |
|---|---|---|---|
| TiC | 570 | Quantum ESPRESSO-GGA | This work |
| | 500 | CASTEP-GGA | [6] |
| | 490 | FPLMTO-LDA | [7] |
| | 57 | Two-body potential | [8] |
| TiN | 354 | Quantum ESPRESSO-GGA | This work |
| | 370 | FPLMTO-LDA | [7] |
| | 364.1 | CASTEP-GGA | [9] |
| | 322.2 | CASTEP-LDA | [9] |
| | 126 | Two-body potential | [8,10] |
| | 310 | Three-body potential | [11] |
| ZrC | 289 | Quantum ESPRESSO-GGA | This work |
| | 295 | CASTEP-GGA | [12] |
| | 98 | Two-body potential | [13] |
| ZrN | 209 | Quantum ESPRESSO-GGA | This work |
| | 205 | CASTEP-GGA | [12] |
| | 94 | Two-body potential | [10] |

Table II. Symmetry, number of atoms per unit cell ($N_a$), structural parameters (a,b,c) and atomic volume (V), and total energy ($E_T$) of the different phases (with associated struktur-bericht designation) of TiC, TiN, ZrC and ZrN at equilibrium. Calculated structural parameters from other experimental (in parentheses) and theoretical (in curly brackets) investigations are also reported.

| Phase | Type | Space Group | No | $N_a$ | a (Å) | b (Å) | c (Å) | V (Å$^3$/atom) | $E_T$ (eV/atom) |
|---|---|---|---|---|---|---|---|---|---|
| TiC | δ-TiC B1 | Fm $\bar{3}$ m Cubic | 225 | 2 | 4.318 (4.318)[a] (4.327)[b] {4.315}[c] | 4.318 | 4.318 | 10.064 | -871.554 |
| | AsNi B8 | P6$_3$/mmc Hexagonal | 194 | 4 | 3.170 | 3.170 | 4.608 | 10.025 | -871.398 |
| | TlI | Cmcm Orthorhombic | 63 | 8 | 2.953 | 8.931 | 3.112 | 10.259 | -871.120 |
| | NiAs B8 | P6$_3$/mmc Hexagonal | 194 | 4 | 3.032 | 3.032 | 5.356 | 10.660 | -871.075 |
| | WC $B_h$ | P $\bar{6}$ m2 Hexagonal | 187 | 2 | 3.054 | 3.054 | 2.656 | 10.727 | -870.888 |
| | CoSn B35 | P6/mmm Hexagonal | 191 | 6 | 4.705 | 4.705 | 3.280 | 10.480 | -870.834 |
| | CsCl B2 | Pm $\bar{3}$ m Cubic | 221 | 2 | 2.700 | 2.700 | 2.700 | 9.842 | -870.402 |
| TiN | δ-TiN B1 | Fm $\bar{3}$ m Cubic | 225 | 2 | 4.232 (4.242)[d] (4.260)[e] {4.230}[c] | 4.232 | 4.232 | 9.474 | -930.261 |
| | ZnS B3 | F $\bar{4}$ 3m Cubic | 216 | 2 | 4.595 | 4.595 | 4.595 | 12.127 | -929.965 |
| | WC $B_h$ | P $\bar{6}$ m2 Hexagonal | 187 | 2 | 2.899 | 2.899 | 2.696 | 9.811 | -929.928 |
| | CsCl B2 | Pm $\bar{3}$ m Cubic | 221 | 2 | 2.636 | 2.636 | 2.636 | 9.158 | -929.368 |
| ZrC | δ-ZrC B1 | Fm $\bar{3}$ m Cubic | 225 | 2 | 4.706 (4.694)[f] (4.730)[g] {4.705}[h] | 4.706 | 4.706 | 13.028 | -752.590 |
| | CsCl B2 | Pm $\bar{3}$ m Cubic | 221 | 2 | 2.946 {2.919}[h] | 2.946 | 2.946 | 12.784 | -751.382 |
| ZrN | δ-ZrN B1 | Fm $\bar{3}$ m Cubic | 225 | 2 | 4.592 (4.585)[i] (4.600)[j] {4.591}[h] | 4.592 | 4.592 | 12.104 | -811.290 |
| | CsCl B2 | Pm $\bar{3}$ m Cubic | 221 | 2 | 2.840 {2.836}[h] | 2.840 | 2.840 | 11.453 | -810.393 |

[a]X-ray powder diffraction file [089-3828]
[b]X-ray powder diffraction file [065-0242]
[c]Ref. [7]
[d]X-ray powder diffraction file [038-1420]
[e]X-ray powder diffraction file [065-0414]

[f]X-ray powder diffraction file [065-0332]
[g]X-ray powder diffraction file [065-0962]
[h]Ref. [12]
[i]X-ray powder diffraction file [078-1420]
[j]X-ray powder diffraction file [065-0961]

Table III. Calculated heat of formation (in eV/formula unit) for TiC, TiN, ZrC, and ZrN based on the B1 (NaCl-type) structure with the corresponding values determined from experiment and other calculations for comparison.

| Phase | $H_f$ (eV/formula unit) | Methodology or Experiment | Reference |
|---|---|---|---|
| TiC | -1.800 | Quantum ESPRESSO-GGA | This work |
| | -1.896 | Experiment | [2] |
| | -1.359 ÷ -1.973 | Experiment | [20] |
| | -1.780 | CASTEP-GGA | [21] |
| TiN | -3.487 | Quantum ESPRESSO-GGA | This work |
| | -3.479 | Experiment | [2] |
| | -3.46 | Experiment | [22] |
| | -3.485 | Experiment | [23] |
| | -3.92 | CASTEP-GGA | [21] |
| | -3.43 | Dmol-GGA | [24] |
| | -3.56 | FLAPW-GGA | [25] |
| ZrC | -1.846 | Quantum ESPRESSO-GGA | This work |
| | -1.912 | Experiment | [2] |
| | -2.08 | Experiment | [26] |
| | -1.72 | VASP-GGA | [27] |
| | -1.82 | FPLMTO-LDA | [28] |
| | -1.64 | VASP-GGA | [29] |
| ZrN | -3.519 | Quantum ESPRESSO-GGA | This work |
| | -3.771 | Experiment | [2] |
| | -3.784 | Experiment | [23] |

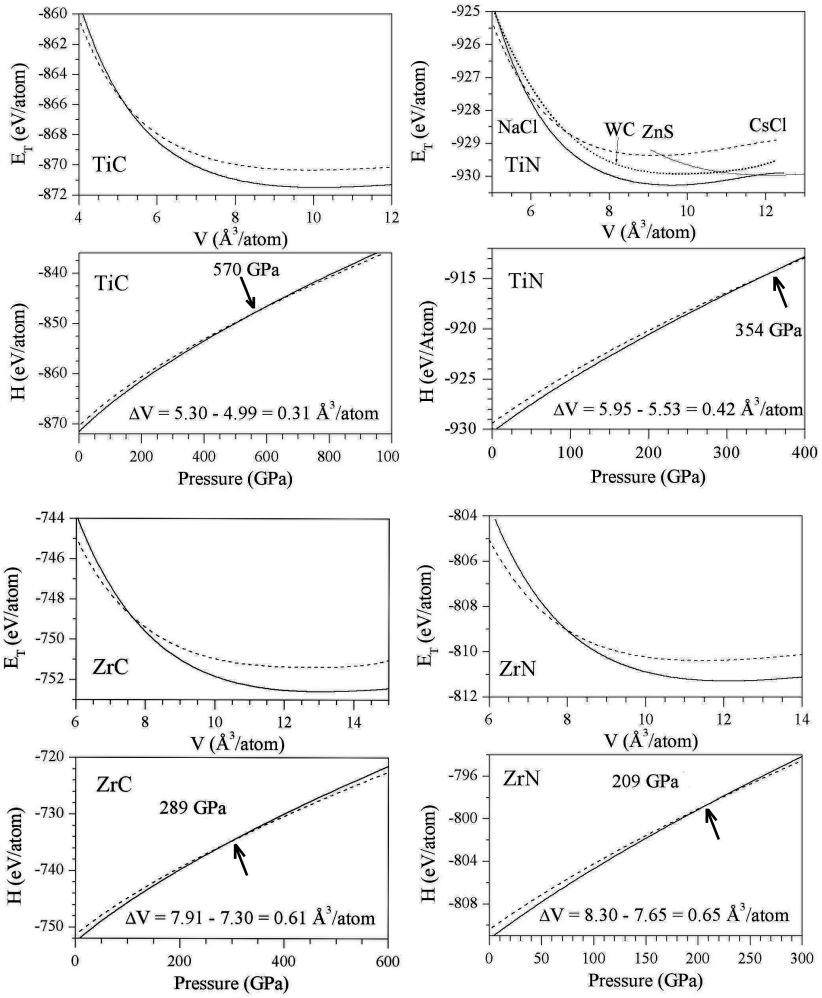


Figure 1. Total energy ($E_T$) as a function of cell volume (V), and enthalpy (H) as a function of pressure for the NaCl (B1)-type (sold line) and CsCl (B2)-type (dashed line) phases of TiC, TiN, ZrC and ZrN. $E_T$(V) and H(P) curves are the result of a six-order polynomial fit to the data points calculated from the first-principles procedure. For TiN, $E_T$(V) for the WC and ZnS -type structures are also reported. ΔV (in Å$^3$/atom) is the volume jump at the transition pressure.

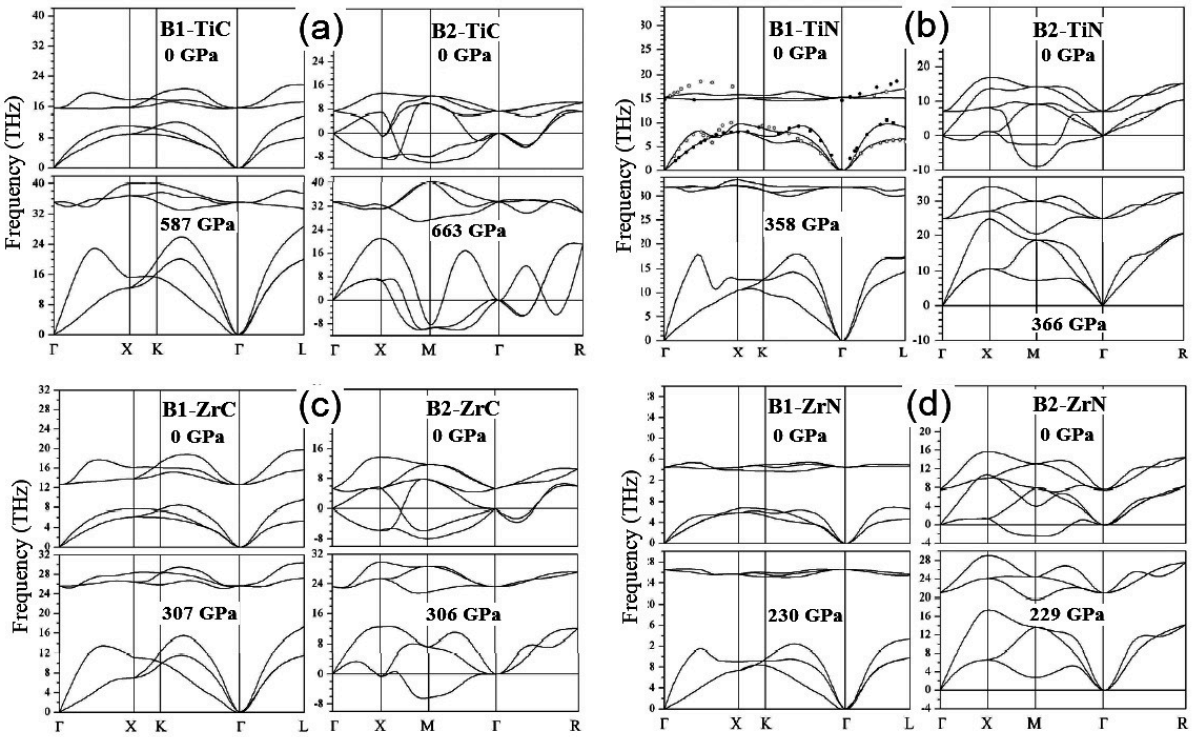


Figure 2. Phonon dispersion curves along some high-symmetry directions of the BZ for the NaCl (B1) and CsCl (B2) -type of (a) TiC, (b) TiN (The points are the experimental results from Ref. [31]), (c) ZrC, and (d) ZrN at equilibrium and under pressure. Note that in some portions of the phonon spectra the "negative" frequencies are "imaginary" (*i.e.*, negative squared frequencies).

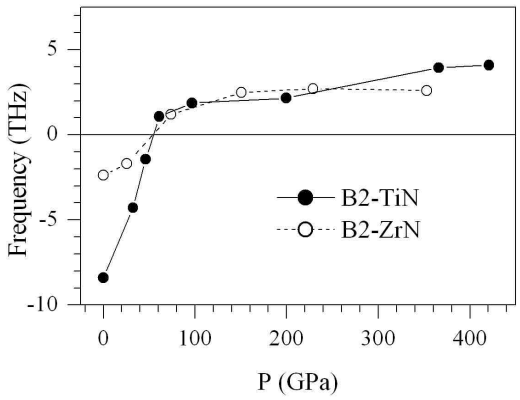


Figure 3. Frequency of the soft acoustic $M_4^-$ mode at the M point as a function of pressure for the CsCl (B2)-type TiN and ZrN.

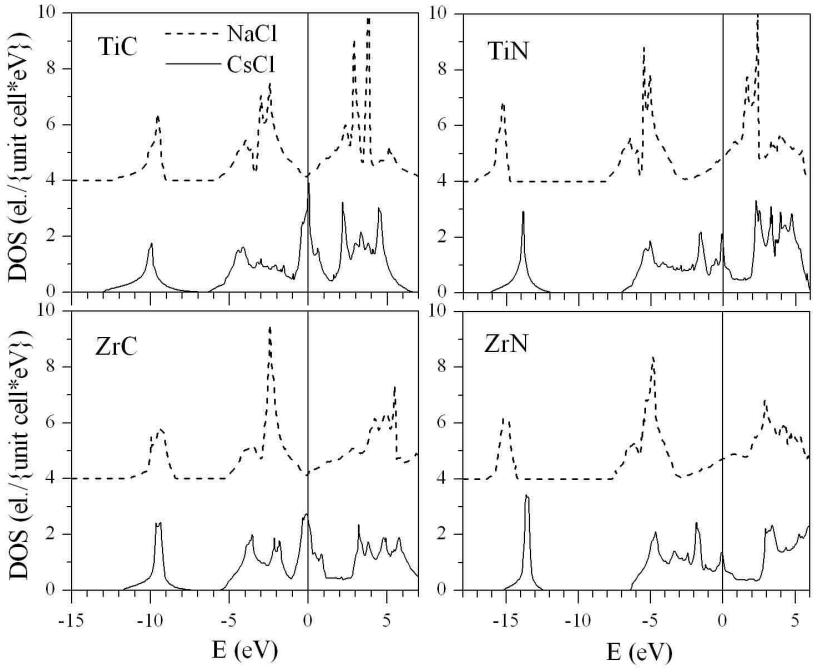


Figure 4. Densities of states (DOS) of the CsCl (B2) (solid line) and NaCl (B1) (dashed line) -type phases of titanium and zirconium carbides and nitrides. The vertical line corresponds to the Fermi level, taken as zero of energy.